



Published in final edited form as:

*Cancer Res.* 2017 October 15; 77(20): 5491–5502. doi:10.1158/0008-5472.CAN-17-0925.

## Human pluripotent stem cell-derived *TSC2*-haploinsufficient smooth muscle cells recapitulate features of Lymphangiomyomatosis

Lisa M. Julian<sup>1,2,\*</sup>, Sean P. Delaney<sup>1,2,3,\*</sup>, Ying Wang<sup>1,\*</sup>, Alexander A. Goldberg<sup>4</sup>, Carole Doré<sup>1</sup>, Julien Yockell-Lelièvre<sup>1</sup>, Roger Y. Tam<sup>1,2,5</sup>, Krinio Giannikou<sup>6</sup>, Fiona McMurray<sup>2,7</sup>, Molly S. Shoichet<sup>5</sup>, Mary-Ellen Harper<sup>2,3,7</sup>, Elizabeth P. Henske<sup>6</sup>, David J. Kwiatkowski<sup>6</sup>, Thomas N. Darling<sup>8</sup>, Joel Moss<sup>9</sup>, Arnold S. Kristof<sup>4</sup>, and William L. Stanford<sup>1,2,3</sup>

<sup>1</sup>Ottawa Hospital Research Institute, Regenerative Medicine Program, Ottawa, ON, Canada

<sup>2</sup>University of Ottawa, Ottawa, ON, Canada

<sup>3</sup>Ottawa Institute of Systems Biology, Ottawa, Ontario, Canada

<sup>4</sup>Research Institute of McGill University Health Centre, Montreal, QC, CA

<sup>5</sup>University of Toronto, Donnelly Centre for Cellular & Biomolecular Research

<sup>6</sup>Division of Pulmonary and Critical Care Medicine, Brigham and Women's Hospital, Harvard Medical School, Boston, MA, USA

<sup>7</sup>Department of Biochemistry, Microbiology and Immunology, Faculty of Medicine

<sup>8</sup>Uniformed Services University of Health Sciences, Bethesda, MD, USA

<sup>9</sup>National Heart, Lung, and Blood Institute, National Institutes of Health, Bethesda, MD, USA

### Abstract

Lymphangiomyomatosis (LAM) is a progressive destructive neoplasm of the lung associated with inactivating mutations in the *TSC1* or *TSC2* tumor suppressor genes. Cell or animal models that accurately reflect the pathology of LAM have been challenging to develop. Here we generated a robust human cell model of LAM by reprogramming *TSC2* mutation-bearing fibroblasts from a patient with both Tuberous Sclerosis Complex (TSC) and LAM (TSC-LAM) into induced pluripotent stem cells (iPSCs), followed by selection of cells that resemble those found in LAM tumors by unbiased *in vivo* differentiation. We established expandable cell lines under smooth muscle cell (SMC) growth conditions that retained a patient-specific genomic *TSC2*<sup>+/-</sup> mutation and recapitulated the molecular and functional characteristics of pulmonary LAM cells. These include multiple indicators of hyperactive mTORC1 signaling, presence of specific neural crest and SMC markers, expression of VEGF-D and female sex hormone receptors, reduced autophagy, and metabolic reprogramming. Intriguingly, the LAM-like features of these cells suggest that haploinsufficiency at the *TSC2* locus contributed to LAM pathology, and demonstrated that iPSC

**Correspondence to:** William L. Stanford, Ottawa Hospital, 501 Smyth Rd, Box 511, Ottawa, ON K1H 8L6 CANADA, Phone: (613) 737-8899 ext. 75495, wstanford@ohri.ca.

\*Equal contribution

reprogramming and SMC lineage differentiation of somatic patient cells with germline mutations was a viable approach to generate LAM-like cells. The patient-derived SMC lines we have developed thus represent a novel cellular model of LAM which can advance our understanding of disease pathogenesis and develop therapeutic strategies against LAM.

### Keywords

cancer susceptibility genes; *TSC2* haploinsufficiency; Lymphangioliomyomatosis; stem cell reprogramming; patient-derived disease models

---

### Introduction

Lymphangioliomyomatosis (LAM, OMIM#606690) is a rare, destructive lung disease associated with inactivating mutations in *TSC1* or, more commonly, *TSC2*. LAM arises either sporadically (S-LAM) or due to germline mutations in association with the multisystem neurodevelopmental and tumor disorder Tuberous Sclerosis Complex (TSC-LAM)(1,2). Found almost exclusively in women, LAM is fundamentally characterized by the progressive growth of microscopic nodules of abnormal smooth muscle-like cells within the lung interstitium, which leads to progressive cystic destruction of the parenchyma, and ultimately respiratory failure(1). The “LAM cells” that grow within these nodules express neural crest lineage markers, predominantly those associated with the smooth muscle cell (SMC) and immature melanocyte lineages, as well as lymphangiogenic proteins and female sex hormone receptors(3–6). LAM patients can also develop renal angiomyolipomas, which similarly express neural crest markers.

*TSC2* encodes a GTPase activating protein that functionally inhibits RHEB, an activator of ‘mechanistic target of rapamycin’ complex 1 (mTORC1), which functions as a central regulator of cell growth, proliferation and survival. Accordingly, *TSC2* loss of function (in complex with *TSC1* and *TBC1D7*) and hyper-activation of mTORC1 are defining features of TSC and LAM(1,2,4). Aside from lung transplantation, the only clinically approved therapy for LAM is treatment with mTORC1 inhibitors (*e.g.*, rapamycin/sirolimus, everolimus), which slow LAM progression but do not eliminate the disease(7). Improved therapeutic options that eliminate or prevent LAM tumors, particularly those aimed at selectively killing LAM cells, are urgently needed.

A major obstacle limiting the development of effective therapies for LAM is a lack of authentic pre-clinical models. Although primary *TSC2*-deficient cells have been isolated from lung biopsies of LAM patients, they cannot be effectively expanded in culture(8). Rodent models of *TSC1/2*-deficiency (*e.g.*, the Eker rat, *TSC1/2*<sup>+/-</sup> mice) do not spontaneously develop LAM lung nodules or cysts, and their uterine and renal tumors do not recapitulate the human disease(8,9). Additionally, primary *TSC2*-deficient cells derived from human patient samples, as well as from many rodent models, typically require viral transformation or p53 deletion for their expansion in culture, and harvested primary tissues are invariably heterogeneous populations of *TSC2*-deficient and -expressing cells(8). It has thus been difficult to establish homogenous cultures of cells that possess the phenotypes of primary LAM cells. While transformed cell lines have been established from a small number

of patient-derived angiomyolipoma tumors(10,11), they do not optimally reflect the genetic background, lineage identity, and molecular characteristics of LAM cells observed in patients.

Induced pluripotent stem cells (iPSCs) have demonstrated tremendous potential for establishing human pre-clinical models of disease, largely because they can be generated from patient-derived somatic cells, are easily expanded, can be induced to differentiate into multiple lineages, and have shown potential in drug screens(12). We reasoned that iPSC reprogramming of TSC-LAM patient fibroblasts and subsequent differentiation into the SMC lineage would be a promising approach for the generation of a LAM cell model. Thus, in the present study, we have established a panel of cell lines that were generated using such a strategy, with dermal fibroblasts from normal-appearing skin and fibroblast-like cells from facial tumors of a TSC-LAM patient(13). These patient-derived cells carry a parental germline *TSC2* mutation and express reduced levels of *TSC2*. They are expandable in culture, and exhibit widespread molecular and phenotypic characteristics that are consistent with LAM cells. Thus, we provide a novel and highly disease-relevant tool for the study of disease mechanisms and identification of novel therapeutic approaches in LAM.

## Materials and Methods

### Cell lines and culture

Fibroblasts were maintained in Dulbecco's modified Eagle medium (DMEM, Thermo Fisher, #11965) containing 10% fetal bovine serum (Gibco, #12483) and 0.5% Penicillin-Streptomycin (Gibco, 15140-122). SMCs were cultured in 231 medium (Thermo Fisher, #M231-500) supplemented with 1× Smooth Muscle Growth Supplement (Thermo Fisher, #S-007-25) and 1× Gentamycin Sulfate (Wisent, #450-135-XL), and in PromoCell phenol red-free Smooth Muscle Cell Basal Medium 2 (C-22267) for starvation growth conditions. Fibroblasts and SMCs were passaged using 0.05% trypsin-EDTA (Gibco, #25300-054). All iPSC and SMC lines used in this study were generated by the authors from fibroblast cultures and were maintained as previously described(14,15). Studies with patient cells were performed following approval by the Stem Cell Oversight Committee (SCOC) of Canada and the IRB (Ottawa Health Science Network-Research Ethics Board REB #2011706-01H), renewed each year of the study, which operates according to the Declaration of Helsinki and the International Ethical Guidelines for Biomedical Research Involving Human Subjects (CIOMS). Fibroblast lines were obtained with informed consent from: as described(13) and by the senior author's laboratory in December 2011 (LAM patient-derived); Coriell Institute (000969), American Type Culture Collection (BJIC), and Progeria Research Foundation (168)(15) in 2009. H9 ESCs were obtained from WiCell Institute in 2004. All cell lines were authenticated by the authors by genotype and/or Western blot analysis for *TSC2*/ tuberin and standard G-banding karyotype analysis (WiCell), and confirmed mycoplasma negative by PCR-based analysis(16). Cryopreserved stocks were established immediately after testing, and experiments were performed within 3–10 passages following thaw of frozen stocks.

### iPSC reprogramming

$1 \times 10^5$  fibroblasts (cultured without antibiotics for 24 hours) were electroporated with 0.5  $\mu\text{g}$  iPSC episomal vector mixture(17) using a 10  $\mu\text{l}$  kit neon transfection system (Thermo Fisher MPK1096) (1300V, 20ms, 2 pulses), and plated into one well of a Matrigel-coated 6-well plate. Cells were cultured in E8 media(18) plus 0.1 $\mu\text{M}$  hydrocortisone until confluency was ~20% (typically 5–10 days), at which point cells were cultured in E7 media (E8 without TGF- $\beta$ ) until PSC colonies were visible (typically 25–30 days post-electroporation). Individual colonies were picked and transferred to Matrigel-coated 24-well dishes and expanded and maintained in E8. For *TSC2*-shRNA transduced fibroblasts: cultures were transferred to E8 + hydrocortisone 48 hours following electroporation.

### In vitro differentiation

For embryoid body (EB)-based differentiation, iPSCs were harvested using 1 mg/mL collagenase IV. Small clumps were transferred to Ultra-low attachment dishes (Corning Inc., Corning, NY) in E6 media (E8 without TGF- $\beta$  and bFGF). Medium was changed every day until EBs had formed (typically 7 days), which were then transferred to gelatin-coated plates and cultured for another 7 days before fixation with 4% formaldehyde.

### Teratoma assay, tissue preparation and harvest

iPSCs were dissociated by dispase (Stem Cell Technologies, Vancouver, Canada), and  $1 \times 10^6$  cells re-suspended in Matrigel were intramuscularly injected into the tibialis anterior muscles of *NOD/SCID* mice (Charles River Laboratory). These studies were approved by the Animal Care Veterinary Services-University of Ottawa (protocol #OHRIT-1666). Once large visible leg tumors had formed (8–11 weeks), teratomas were dissected and representative tissue was either fixed in 4% formaldehyde and embedded in paraffin, or manually dissociated. Paraffin-embedded tissues were sectioned and stained with hematoxylin and eosin or by immunohistochemistry. To isolate and expand SMCs in culture, manually dissociated tissue was further dissociated with trypsin-EDTA at 37°C for 20 min, washed and centrifuged at 1000 rpm for 10 min, and cultured for multiple passages in SMC growth media on tissue culture treated plastic or Matrigel (for isolation and early passages only).

### shRNA-mediated TSC2 knock-down

Fibroblasts and SMCs were transduced with dual-cistronic lentiviral vectors engineered to express both turboGFP and human *TSC2*-targeted (or scrambled control [Control]) shRNA sequences in the presence of doxycycline (GE Dharmacon SmartChoice lentiviral line; *TSC2*-sh1, VSH6376-220794900; *TSC2*-sh2, VSH6376-220794908; Scrambled control, VSC6572). shRNA expression was induced by adding freshly dissolved 500  $\mu\text{g}/\text{mL}$  (fibroblasts) or 1 mg/mL (SMCs) doxycycline to the culture media for a minimum of 7 days prior to iPSC reprogramming or harvest/ analysis. shRNA expression was maintained throughout the entire course of reprogramming.

### Extracellular flux assays

Oxygen consumption and extracellular acidification rates (OCR and ECAR, respectively) were measured using a Seahorse XF-24 bioanalyzer (Agilent Technologies).  $6.5 \times 10^4$  live cells were plated per well in a Matrigel-coated 24-well dish (Agilent, 100882-004) 18–24 hours prior to experiments. Concentrations of molecules used in the mitochondrial stress test and glycolysis assays were as follows: FCCP (1  $\mu$ M), oligomycin (1  $\mu$ g/mL), antimycin A (1  $\mu$ M), rotenone (0.5  $\mu$ M), glucose (10 mM), 2-deoxyglucose (100 mM). OCR and ECAR were normalized to total cell protein; OCR was also corrected for non-mitochondrial respiration.

### mTORC1 and autophagy inhibitor treatments

For rapamycin and chloroquine experiments, SMCs were cultured in SMC growth media until ~60% confluent and were treated with 10 nM rapamycin (Calbiochem, #553211), 5  $\mu$ M chloroquine (Sigma, #C6628), or vehicle (DMSO at 1/1000) in basal DMEM (Gibco, #11054-020) for 24 hrs. Cells were then harvested for flow cytometry analysis (for each sample, media- and trypsin-harvested adherent cells were combined). Cells were stained with propidium iodide (PI) (50 ng per  $5 \times 10^4$  –  $1 \times 10^5$  cells) and analyzed for PI staining *via* flow cytometry. For bafilomycin A1, torin-1, rapamycin experiments: cells were treated with 2 nM torin-1 (Millipore, #475991), 50 nM rapamycin (or DMSO for controls) for 4 hours, and then with 250 nM bafilomycin A1 (or DMSO for controls) (Enzo Life Sciences, # BML-CM110-0100) for an additional 2 hours. Cells were then harvested into protein lysis buffer for western blot analysis.

### Statistical analysis

Statistical analyses to assess differences across groups were performed using one-way analysis of variance (ANOVA) or two-tailed student's t-test, where indicated. Where ANOVA analysis revealed significant differences, a Tukey post hoc test was used for pairwise comparisons. Error bars represent standard error of the mean. P values of <0.05 (\*), <0.01 (\*\*), and <0.001 (\*\*\*) were considered statistically significant.

Additional information can be found in Supplementary Materials and Methods.

## Results

### Generation and characterization of TSC-LAM patient-derived iPSCs

Low-passage dermal fibroblasts were grown from explants from either facial tumor tissue or normal-appearing skin (tissue adjacent to visible tumors) obtained from two women with TSC and clinical manifestations of LAM. Next generation sequencing revealed that Patient 6 (P6) carries a *TSC2* germline mutation with two additional second-hit *TSC2* mutations in her angiofibroma-derived fibroblasts, each with allele frequency of less than 0.5 (Supplementary Fig. S1A and (13)). Thus, cultures of normal-appearing fibroblasts ('Norm-fib') from P6 can be expected to be a homogenous *TSC2*<sup>+/-</sup> population. Tumor-derived fibroblasts ('Tum-fib') from P6 are likely composed of both *TSC2*<sup>-/-</sup> and, as confirmed later, *TSC2*<sup>+/-</sup> cells (Fig. 1A). Mutation analysis of blood and fibroblasts grown from Patient 5 (P5) demonstrated that the patient was mosaic for a first-hit *TSC2* mutation, with allele

frequency of 0.07 in blood(13). Three tumor-derived fibroblast lines from P5 had second-hit point mutations or deletions at varying allele frequencies (Supplementary Fig. S1A and (13)). Cultures from P5 are therefore expected to be heterogeneous mixtures of either  $TSC2^{+/+}$ ,  $TSC2^{+/-}$  ('Norm-fib') or  $TSC2^{+/+}$ ,  $TSC2^{+/-}$ ,  $TSC2^{-/-}$  ('Tum-fib' lines) cells (Fig. 1A). Consistent with TSC2-deficiency and concomitant mTORC1 hyper-activation in tumor-derived cells, TSC2 protein expression was substantially reduced and levels of phosphorylated S6 (P-S6) were elevated in all tumor cell lines compared to the normal-appearing fibroblasts for each patient (Supplementary Fig. S1B and (13)).

To determine whether TSC-LAM somatic cells are able to acquire a pluripotent state, patient-derived fibroblast lines were subjected to epigenetic reprogramming. Morphological changes suggestive of mesenchymal-to-epithelial transition were noticeable by day 5 post-transduction, and colonies resembling those formed by human embryonic stem cells (hESCs) were visible by days 20–25. hESC-like colonies were obtained from all sources except for the P5 angiofibroma Nose-Tum-fib cells (Fig. 1A). A subset of colonies was manually harvested and sub-cultured in individual Matrigel-coated wells at day 30 post-transduction, and these have now maintained an undifferentiated hESC-like morphology for over 25 passages (Fig. 1B). We randomly selected 2–3 clones from each group and performed standard iPSC characterization assays. Most lines possessed a karyotype identical to that of the parental fibroblasts (Supplementary Fig. S2A&B; lines with abnormal karyotypes were excluded from further study), all lines expressed classical pluripotency markers (Fig. 1C, Supplementary Fig. S3A&B), and most were capable of differentiating into cells that express markers of all three germ layers *in vitro* and *in vivo* (Supplementary Fig. S3A–E). The one exception is that P6 tumor-derived iPSCs were unable to generate GATA6<sup>+</sup> endoderm lineage cells.

### TSC2-deficiency inhibits iPSC reprogramming

In all but one case (P5 'FH-Tum-fib') the tumor-derived fibroblasts gave rise to fewer colonies than did the normal-appearing dermal cells from each patient (Fig. 1A), suggesting that complete loss of TSC2 represents a barrier to somatic cell reprogramming to pluripotency. Genotyping analysis revealed that while all iPSC colonies derived from P6 carried the first-hit  $TSC2$  germline mutation found in the parental cell lines ( $TSC2$  c. 4375C>T, p.R1459\*), none of the second-hit mutations observed in the tumor-derived fibroblasts were present (Supplementary Fig. S4A&B). Thus, the P6 iPSC lines are genotypically  $TSC2^{+/-}$ ; accordingly, they each express  $TSC2$  at half-maximal levels compared to wild type (WT) controls (Fig. 1D). No  $TSC2$  mutations were identified in colonies derived from the mosaic dermal cultures of P5 (Supplementary Fig. S4B&C).

We attempted to reprogram two additional cell sources that are widely considered to be TSC2-deficient: the human renal angiomyolipoma-derived 621-101 cell line(11) and primary LAM patient lung explants isolated at the time of double lung transplant. The latter typically yield  $TSC2$  genetically heterogenous cultures. The 621-101 cells gave rise to partially reprogrammed colonies that were unstable and could not be re-established from cryopreserved samples. All iPSC lines generated from the lung explants demonstrated normal TSC2 (and TSC1) expression. To directly test the hypothesis that TSC2-deficiency



inhibits reprogramming, we used a doxycycline (Dox)-inducible shRNA approach to knock down *TSC2* in otherwise normal fibroblasts and performed subsequent iPSC reprogramming experiments. As expected, reduction of *TSC2* expression to 36–45% of normal levels (Fig. 1E) resulted in a substantially reduced number of reprogrammed iPSC colonies (Fig. 1F).

### Establishment of TSC-LAM patient-derived smooth muscle cells

Considering the possibility that iPSC lines derived from tumor biopsies may have retained an epigenetic memory of their original tumor microenvironment(19), we tested whether the normal dermal- and tumor-derived iPSCs adopt distinct cellular phenotypes upon *in vivo* differentiation. We injected representative tumor and normal tissue-derived iPSCs from P5 (*TSC2<sup>+/+</sup>*) and P6 (*TSC2<sup>+/-</sup>*), as well as control iPSCs derived from individuals without TSC or LAM, into immunodeficient mice for teratoma growth and subsequent analysis of differentiated tissues. All iPSC lines gave rise to teratomas over a similar time-frame, and grew to a similar size with comparative multipotent differentiation potential (Supplementary Fig. S3D&E).

Given a potential pathogenic role for *TSC2<sup>+/-</sup>* cells in TSC and LAM lesions(20–23), we focused on two tumor-derived (P6T1, P6T2) and two normal-appearing dermal-derived (P6N1, P6N2) P6 *TSC2<sup>+/-</sup>* iPSC lines. Overall, these cell lines demonstrate elevated mTORC1 signaling, evidenced by increased phosphorylation of S6 kinase (P-S6K) compared to WT non-patient iPSC controls (969B and 168) (Fig. 2A). We reasoned that it may be possible to isolate disease-relevant LAM cells by culturing tumor explants under growth conditions selective for the putative cell type of interest. Given the pervasive expression of SMC markers in LAM lung and kidney lesions, we predicted that isolation of teratoma-derived SMCs would select for LAM-like cells. To investigate this, we cultured a portion of each P6-derived teratoma directly under SMC growth conditions (Fig. 2B). Robust cell cultures morphologically similar to SMCs were quickly established from the P6 teratoma-derived tissue (Fig. 2C) (designated fibroblast tumor-derived lines P6T1-SMC and P6T2-SMC, and normal dermal tissue-derived lines P6N1-SMC and P6N2-SMC; Fig. 2B). WT control SMC lines were established by culturing a representative portion of teratoma tissue derived from non-TSC/LAM 00969B iPSCs (120lb-SMC, 120ls-SMC, 121-SMC; Fig. 2B), or *via* directed *in vitro* differentiation of iPSCs into the SMC lineage (BJ1C-SMC; Fig. 2B)(24). P6-derived cultures maintain SMC-like morphology and growth potential similar to control SMC cultures in excess of 20 passages (greater than 50 population doublings), importantly without requiring viral transformation. Each P6-SMC line expresses the classical smooth muscle cell marker Smooth Muscle Actin (SMA) at levels comparable to WT controls and the 621-101 cell line (cultured under the same growth conditions; Fig. 2D&E), as determined by quantitative high content imaging (HCI). Importantly, *TSC2* protein expression is reduced in P6-SMCs, in each case falling at a level in between WT control and *TSC2<sup>-/-</sup>* 621-101 cells (Fig. 2D, F, G). *TSC2* mRNA expression is reduced in P6-SMCs to 23–63% that of control cells (Fig. 2H).

The reduced levels of *TSC2* mRNA and protein in the P6-SMC lines suggests that they have maintained the heterozygous *TSC2* status observed in the iPSC state. Sanger, Snapshot and next generation sequencing confirmed the 4375C>T mutation (Fig. S1A) at 50% allele

frequency in all P6-SMC lines. We tested the possibility that second-hit mutations were acquired during teratoma development, however our multiple sequencing methods failed to detect any additional *TSC2* mutations or any mutations among a bait set of 49 genes related to the TSC/mTOR pathway. Thus, the P6-SMC lines are genetically similar to the iPSC lines from which they were derived, each carrying the same patient-derived *TSC2* germline mutation.

### Patient-derived SMCs exhibit markers of mTORC1 activation

Next, we examined the SMC lines for indicators of hyperactive mTORC1 signaling (Fig. 3A). In P6-SMCs we observed elevated P-S6K to varying degrees and a consequent increase in cell size, classical markers of mTORC1 activation(1,25) (Fig. 3B&C). Cells in which *TSC2* expression was further reduced by Dox-inducible shRNA targeting exhibited a greater increase in size (Supplementary Fig. S5A–C), suggesting that the *TSC2*<sup>+/-</sup> SMCs display an intermediate response to mTORC1 activation. Also reflecting elevated mTORC1 signaling and *TSC2*-deficiency(26), we observed impaired autophagic flux in P6-SMCs, indicated by reduced accumulation of the lipidated form of LC3B (LC3B-II) in the presence of the lysosomal acidification inhibitor bafilomycin A1 (Fig. 3D). HIF1 $\alpha$  protein levels were elevated in a subset of P6-SMC lines compared to control cells (Fig. 3E) and, as expected, were attenuated by treatment with the mTORC1 inhibitor rapamycin (Fig. 3F). Thus, *TSC2*<sup>+/-</sup> P6-SMCs demonstrate canonical features of hyperactive mTORC1 signaling.

### Patient-derived SMCs exhibit known biomarkers of LAM

Pulmonary LAM cells express neural crest lineage markers, including the melanoma-associated antigens ganglioside D3 (GD3) and glycoprotein 100 (gp100), identified by HMB45 antibody (4,27–31). We find that under serum starvation conditions, where mTORC1 activity should normally be repressed, tumor-derived and P6N2-SMC lines express GD3 at a high frequency (48–56% GD3<sup>+</sup>), whereas WT control SMC or 621-101 cultures have substantially fewer GD3<sup>+</sup> cells (8–15% GD3<sup>+</sup>) (Fig. 4A&B). Immunofluorescence for gp100 revealed a typical cytoplasmic, largely punctate staining pattern in a minority of cells in P6-SMCs (Supplementary Fig. S6A); gp100 was also detected *via* immunohistochemistry in a subset of cells (Supplementary Fig. S6B). Low staining in 621-101s was also observed, and while visibly higher in P6-SMCs compared to WT and non-specific antibody control conditions, gp100 staining intensity did not substantially increase in response to further reduction of *TSC2* expression in P6-SMCs (Supplementary Fig. S6A). This low and heterogenous level of staining in the proliferative P6-SMC cultures may reflect the inverse correlation between gp100 and PCNA levels (*i.e.*, proliferation) previously observed in LAM nodules (29,31–33).

Intriguingly, in P6-SMCs levels of the lymphangiogenic factor VEGF-D, an important diagnostic biomarker for LAM (34,35), were two-fold higher than in controls (Fig. 4C). Reduced levels of  $\beta$ -Catenin were also observed in both the 621-101 and P6-SMC lines (Fig. 4D), a phenotype recently reported in *TSC2*-deficient melanocytes (36). Consistent with the female preponderance of LAM, P6-SMCs exhibited pervasive expression of Progesterone Receptor (PR) and Estrogen Receptor alpha (ER- $\alpha$ ) (3–6) (Fig.4E), which notably did not appear to change with further *TSC2* reduction (Supplementary Fig. S6C). Thus, P6-SMCs



exhibit the majority of molecular phenotypes found in LAM cells *in situ*, notably to a greater degree than the 621-101 angiomyolipoma-derived cell line (Table 1).

### Glycolytic metabolic reprogramming in *TSC2*<sup>+/-</sup> SMCs

Like cancer cells, *TSC2*-deficient cells are characterized by an atypical dependence on glycolytic metabolism at the expense of mitochondrial oxidative phosphorylation (4,37,38). Reflecting this, P6-SMC lines exhibited increased expression of the glycolytic enzymes *GLUT1*, enolase, and *G6PDH* compared to both WT controls and 621-101 cells (Fig. 5A–C). Importantly, *G6PDH* is associated with flux through the pentose phosphate pathway, a phenotype previously associated with *TSC2*-deficient cells (39). Correspondingly, levels of the *PGC1a* transcription factor, which is indicative of flux through the mitochondrial electron transport chain (ETC), were substantially reduced in the P6 tumor-derived and P6N2 SMC lines (Fig. 5D).

To directly test for a glycolytic phenotype in P6-SMCs, we performed a series of cellular energetics assays designed to test responses to stimulation or perturbation of mitochondrial and glycolytic metabolic pathways. Compared to P6-SMCs, control cell lines exhibited a higher resting oxygen consumption rate (OCR) as well as an increased maximal respiratory capacity (OCR in the presence of the ATP synthase inhibitor oligomycin and ETC chemical uncoupler FCCP) (Fig. 5E). This is due to a higher ATP production in control lines (based on reduction in OCR levels following the addition of oligomycin) (Fig. 5F). We observed a significantly higher extracellular acidification rate (ECAR) in the P6N2 and tumor-derived SMC lines compared to controls under both glucose-free and glucose-stimulated conditions; ECAR was also elevated in P6-SMC lines following ATP synthase inhibition (Fig. 5G). Thus, P6-SMCs exhibit an increased glycolytic metabolic phenotype, in contrast to the aerobic state of WT control cells.

### Combined autophagy and mTORC1 inhibition selectively sensitizes tumor-derived SMCs to cell death

Cellular macroautophagy is tightly regulated by mTORC1 activity, leading to speculation that the cytostatic but non-cytotoxic effects of rapamycin on LAM cells is due to enhanced autophagy via metabolic reprogramming (1,4,40). Indeed, a degree of dependency on autophagy for cell survival in the context of rapamycin treatment has been demonstrated *in vivo* using both xenograft and transgenic mouse *TSC* models (26). We found reduced autophagic flux in P6-SMCs (Fig. 3D), and show here that basal LC3B-II levels become elevated in these cells when mTOR is inhibited by rapamycin or torin-1 (Fig. 6A&B). This suggests that autophagy is regulated in an mTORC1-dependent manner in P6-SMCs, and specifically that autophagy is elevated in these cell lines in the presence of mTORC1 inhibitors.

We next sought to address whether these autophagy signaling dynamics could be exploited in a therapeutic context to selectively kill these cells in combination with rapamycin treatment, as has been previously shown in the murine *TSC2*-deficient ELT3 cell line (26). To test this strategy, we treated WT control, 621-101, and P6-SMC lines with rapamycin and the autophagy inhibitor chloroquine, either alone or in combination, and assessed cell death

24 hours later. First, P6-SMCs exhibited increased viability under basal growth conditions compared to controls (Supplementary Fig. S7). Culturing these cells for 24 hours in serum- and nutrient-deficient (“starved”) media did not affect cell viability on its own (Supplementary Fig. S7). Moreover, treatment with either rapamycin or chloroquine alone under starved conditions did not significantly reduce viability in any of the lines tested (Fig. 6C). Combination treatment with rapamycin and chloroquine, however, resulted in a significant increase in cell death in the P6 tumor-derived SMC lines, but not those lines derived from the P6 normal tissue, WT control lines, or 621-101 cells (Fig. 6C). Thus, patient tumor-derived SMC lines have specifically retained an autophagy-dependent survival mechanism that is activated upon mTORC1 inhibition.

## Discussion

Through epigenetic reprogramming, *in vivo* differentiation, and subsequent SMC lineage selection of dermal cells derived from a TSC-LAM patient, we have generated expandable, non-transformed, human cell lines carrying a *TSC2* mutation that exhibit multiple characteristics of classical LAM cells (summarized in Table 1). In addition to modeling LAM, our work has revealed key features of the role of TSC2 in establishing pluripotency. P6 dermal cultures, which contained both *TSC2*<sup>+/-</sup> and *TSC2*<sup>-/-</sup> cells, only gave rise to *TSC2*<sup>+/-</sup> iPSCs, and the mosaic P5 dermal cultures established only *TSC2*<sup>+/+</sup> colonies. These observations suggest that, within a bulk population those cells that express the highest levels of TSC2 will out-compete others in establishing pluripotent colonies, and further that cells completely devoid of TSC2 are incapable of epigenetic reprogramming to the pluripotent state. These findings are consistent with previous observations that hyperactive mTORC1 signaling is a barrier to iPSC reprogramming in mice, a phenomenon linked to a precise regulation of macroautophagy (41,42), and establish TSC2 as an important mediator of reprogramming to pluripotency. It is particularly notable that *TSC2*<sup>+/-</sup> iPSC colonies exhibit an increased propensity toward genomic instability (3 of 7 P6 *TSC2*<sup>+/-</sup> iPSC lines exhibited abnormal karyotypes, compared to only 2 of 12 iPSC lines derived from P5 and 00969 *TSC2*<sup>+/+</sup> dermal cells; Supplementary Fig. S2A&B). Additionally, P6 tumor-derived iPSCs were unable to establish GATA6<sup>+</sup> endoderm cells *in vitro* (although endoderm-like tissue was observed *in vivo*) (Supplementary Fig. S3A&D). In our extensive experience with iPSC culture and reprogramming using cells derived from both unaffected individuals and those with various genetic diseases, we have never before observed karyotypic and developmental abnormalities to this magnitude (14,43–46). Together, these data suggest that TSC2 is required for reprogramming to pluripotency and that, while a half-maximal level of TSC2 is sufficient to establish iPSC colonies it sensitizes cells to atypically high levels of reprogramming-related stress. Strikingly, unpublished observations in our lab with *TSC2*-knockout hESCs generated by genome editing have revealed that TSC2 is not similarly required to maintain pluripotency.

Consistent with other cellular models of LAM, P6-SMCs exhibit enhanced mTORC1 signaling, likely secondary to reduced TSC2 (11). However, compared to other models, which notably are fully *TSC2*-deficient (*TSC2*<sup>-/-</sup>) but were not derived under SMC growth conditions (11), P6-N2 and tumor-derived SMCs express an increased number of mTOR- and LAM-associated features, including neural crest differentiation markers (e.g., GD3) and

lymphangiogenesis biomarkers (VEGF-D) (Table 1). Additionally, tumor-derived lines are uniquely sensitive to combined mTORC1 and autophagy inhibition (Table 1). These differences strongly suggest that selection of *TSC2* mutation-bearing cells under SMC growth conditions promotes the isolation and expansion of cells with potent LAM-like phenotypes, whether they be *TSC2*<sup>+/-</sup> or *TSC2*<sup>-/-</sup>. This highlights the importance of employing the appropriate supportive culture conditions to promote the selection and expansion of desired cell types (typically tumor and disease-related cells) from heterogeneous populations. The LAM-associated phenotypes observed in P6-SMC cultures, including expression of the melanocyte marker GD3, supports the hypothesis that LAM cells are associated with the neural crest-SMC lineage (29,47,48). Given that the TSC-LAM patient-derived teratomas exhibited multi-lineage differentiation, it is foreseeable that cell types associated with other TSC-associated lesions, specifically the neural and broader neural crest lineages (1), may be isolated by culturing patient iPSC-derived teratoma tissue under culture conditions supportive of these lineages.

Intriguingly, *TSC2*<sup>+/-</sup> P6-SMCs demonstrate haploinsufficiency, as they exhibit a majority of the molecular, morphological and metabolic features attributed to LAM cells, which are typically considered to be *TSC2*-null. Thus, it is possible that *TSC2*<sup>+/-</sup> cells may potentiate disease phenotypes within LAM nodules. Our observations align with recent studies showing that *TSC2*<sup>+/-</sup> cells can exhibit some disease-associated phenotypes and may contribute to pathology in TSC and LAM (20–23), and that *TSC2*-expressing cells can acquire aberrant phenotypes when associated with *TSC2*-deficient cells (49). It is important to note, however, that while some phenotypes were unchanged (e.g., gp100 and ER- $\alpha$  expression) (Supplementary Fig. S6), further reduction of *TSC2* in P6-SMCs led to a substantial elevation in LAM-associated mTORC1 activity (Supplementary Fig. S5); thus, the full extent of LAM-associated phenotypes might only be observed in *TSC2*<sup>-/-</sup> cells. In agreement, while results were similar across all four P6-derived cell lines for most of the mTOR- and LAM-associated assays we conducted, some phenotypes were apparent in only a subset of the P6-SMC lines (e.g., elevated HIF1 $\alpha$  and GD3 expression, specific metabolic features). Additionally, while combined rapamycin and chloroquine treatment caused toxicity in tumor-derived SMC lines, these effects were relatively modest (Fig. 6C). Thus, while *TSC2*<sup>+/-</sup> SMCs show potential utility in drug screens aimed at identifying molecules that selectively kill LAM cells, *TSC2*<sup>-/-</sup> SMCs will likely be optimal, underscoring the need for the establishment of *TSC2*-knockout cell lines via approaches such as genomic engineering.

Although P6-SMC lines appear to be genetically identical based on our sequencing analyses, the tumor-derived lines express some phenotypes not observed in the normal dermal-derived lines, most notably sensitivity to combined mTORC1 and autophagy inhibition. Thus, it seems likely that the P6 tumor-derived SMCs have retained some epigenetic memory, a phenomenon previously documented in reprogrammed iPSC lines (19), that is associated with their original identity as tumor cells. This suggests that tumor-derived cells, and likely also those that are *TSC2*-null, are most appropriate for establishing TSC- and LAM-like cell lines suitable for disease modeling and drug screening studies. Additionally, only the P6T1-SMC line exhibited all LAM-like features that we evaluated, while other lines lacked 1–3 key features. This highlights a moderate level of clone-specific phenotypic variability and,

consequently, the importance of screening multiple clones in patient-derived cell panels to identify the best candidates. However, as our four P6-SMC lines are still highly similar to one another, we believe our approach represents a robust and reproducible method of establishing disease-relevant cell lines.

In summary, we have used iPSC technology to shed light on the developmental and genetic events required for the evolution of LAM cells and tumors. In doing so, we have developed a novel and relevant patient-derived cell model of LAM, as well as a unique technical approach to selecting and expanding *TSC2* mutation-bearing LAM-like cells. TSC-mTORC1 signaling is a central component of the physiology of all cells and is involved in a multitude of developmental processes (1,50). Accordingly, dysregulation of this pathway is implicated in a number of cancer syndromes and human diseases (50). Thus, our findings of essential roles of TSC2 in establishing pluripotency and in driving (LAM) disease-related phenotypes in a (SMC) lineage-dependent manner have broad implications for our understanding of both development and cell fate regulation, and offer important insights for the generation of additional human cell-based models of disease.

## Supplementary Material

Refer to Web version on PubMed Central for supplementary material.

## Acknowledgments

We wish to thank Kamal Garcha for his early work on this project and Catherine Lawrence for her inspiration. We would also like to thank the RI-MUHC Histopathology Platform for their help.

**Financial support:** This research was supported by a Special Accelerated Discovery grant by the McEwen Centre for Regenerative Medicine, supported by Green Eggs and LAM to W.L. Stanford and M.S. Shoichet and a grant (W81XWH-14-1-0434) awarded to W.L. Stanford and A.S. Kristof from the United States Department of Defense *via* the Tuberous Sclerosis Complex Research Program of the Congressionally Directed Medical Research Program. Salary support for Y. Wang, A. Goldberg, C. Doré, J. Yockell-Lelièvre, and R.Y. Tam was provided through these grants. Research reported in this publication was additionally supported by the National Institute of Arthritis and Musculoskeletal and Skin Diseases of the National Institutes of Health (NIH) (award #R01AR062080) to T.N. Darling, the Canadian Institutes of Health Research (CIHR) (FDN 143278) to M. Harper, and the Intramural Research Program, NIH, National Heart, Lung, and Blood Institute (J. Moss). We are grateful for support from the LAM Foundation and LAM Canada (A.S. Kristof), and from the Lucy J Engles TSC/LAM Research Program (E.P. Henske and D.J. Kwiatkowski). L.M. Julian was supported by Ontario Institute for Regenerative Medicine and CIHR Banting Postdoctoral Fellowships; S.P. Delaney by a Judith R. Raymond Scholarship in Cancer Research; A. Goldberg by a Richard and Edith Strauss Fellowship in Respiratory Medicine; F. McMurray by a Destination 2020 University of Ottawa and Ontario Ministry of Research Fellowship. W.L. Stanford was funded by a Tier 1 Canada Research Chair in Integrative Stem Cell Biology.

## References

1. Delaney SP, Julian LM, Stanford WL. The neural crest lineage as a driver of disease heterogeneity in Tuberous Sclerosis Complex and Lymphangioleiomyomatosis. *Front Cell Dev Biol.* 2014; 2:69. [PubMed: 25505789]
2. Henske EP, Jozwiak S, Kingswood JC, Sampson JR, Thiele EA. Tuberous sclerosis complex. *Nat Rev Dis Primers.* 2016; 2:16035. [PubMed: 27226234]
3. Grzegorek I, Lenze D, Chabowski M, Janczak D, Szolkowska M, Langfort R, et al. Immunohistochemical evaluation of pulmonary lymphangioleiomyomatosis. *Anticancer Res.* 2015; 35:3353–60. [PubMed: 26026095]
4. Henske EP, McCormack FX. Lymphangioleiomyomatosis - a wolf in sheep's clothing. *J Clin Invest.* 2012; 122:3807–16. [PubMed: 23114603]

5. Gao L, Yue MM, Davis J, Hyjek E, Schuger L. In pulmonary lymphangioliomyomatosis expression of progesterone receptor is frequently higher than that of estrogen receptor. *Virchows Archiv*. 2014; 464:495–503. [PubMed: 24570392]
6. Logginidou H, Ao X, Russo I, Henske EP. Frequent estrogen and progesterone receptor immunoreactivity in renal angiomyolipomas from women with pulmonary lymphangioliomyomatosis. *Chest*. 2000; 117:25–30. [PubMed: 10631194]
7. Ando K, Kurihara M, Kataoka H, Ueyama M, Togo S, Sato T, et al. Efficacy and safety of low-dose sirolimus for treatment of lymphangioliomyomatosis. *Respir Investig*. 2013; 51:175–83.
8. Darling TN, Pacheco Rodriguez G, Gorio A, Lesma E, Walker C, Moss J. Lymphangioliomyomatosis and TSC2  $-/-$  Cells. *Lymphatic Research and Biology*. 2010; 8:59–69. [PubMed: 20235888]
9. Kwiatkowski DJ. Animal models of lymphangioliomyomatosis (LAM) and tuberous sclerosis complex (TSC). *Lymphatic Research and Biology*. 2010; 8:51–7. [PubMed: 20235887]
10. Arbiser JL, Yeung R, Weiss SW, Arbiser ZK, Amin MB, Cohen C, et al. The generation and characterization of a cell line derived from a sporadic renal angiomyolipoma: use of telomerase to obtain stable populations of cells from benign neoplasms. *The American Journal of Pathology*. 2001; 159:483–91. [PubMed: 11485907]
11. Yu J, Astrinidis A, Howard S, Henske EP. Estradiol and tamoxifen stimulate LAM-associated angiomyolipoma cell growth and activate both genomic and nongenomic signaling pathways. *Am J Physiol Lung Cell Mol Physiol*. 2004; 286:L694–700. [PubMed: 12922981]
12. Avior Y, Sagi I, Benvenisty N. Pluripotent stem cells in disease modelling and drug discovery. *Nat Rev Mol Cell Biol*. 2016; 17:170–82. [PubMed: 26818440]
13. Tyburczy ME, Wang J-A, Li S, Thangapazham R, Chekaluk Y, Moss J, et al. Sun exposure causes somatic second-hit mutations and angiofibroma development in tuberous sclerosis complex. *Hum Mol Genet*. 2014; 23:2023–9. [PubMed: 24271014]
14. Chang WY, Lavoie JR, Kwon SY, Chen Z, Manias JL, Behbahani J, et al. Feeder-independent derivation of induced-pluripotent stem cells from peripheral blood endothelial progenitor cells. *Stem Cell Res*. 2013; 10:195–202. [PubMed: 23291290]
15. Chen Z, Chang WY, Etheridge A, Strickfaden H, Jin Z, Palidwor G, et al. Reprogramming progeria fibroblasts re-establishes a normal epigenetic landscape. *Aging Cell*. 2017; 16:870–87. [PubMed: 28597562]
16. Uphoff CC, Drexler HG. Detection of mycoplasma contaminations. *Methods Mol Biol*. 2005; 290:13–23. [PubMed: 15361652]
17. Okita K, Matsumura Y, Sato Y, Okada A, Morizane A, Okamoto S, et al. A more efficient method to generate integration-free human iPSC cells. *Nat Methods*. 2011; 8:409–12. [PubMed: 21460823]
18. Chen G, Gulbranson DR, Hou Z, Bolin JM, Ruotti V, Probasco MD, et al. Chemically defined conditions for human iPSC derivation and culture. *Nat Methods*. 2011; 8:424–9. [PubMed: 21478862]
19. Kim K, Doi A, Wen B, Ng K, Zhao R, Cahan P, et al. Epigenetic memory in induced pluripotent stem cells. *Nature*. 2010; 467:285–90. [PubMed: 20644535]
20. D'Armiento J, Shiomi T, Marks S, Geraghty P, Sankarasharma D, Chada K. Mesenchymal Tumorigenesis Driven by TSC2 Haploinsufficiency Requires HMGA2 and Is Independent of mTOR Pathway Activation. *Cancer Res*. 2016; 76:844–54. [PubMed: 26837766]
21. Wilson C, Bonnet C, Guy C, Idziaszczyk S, Colley J, Humphreys V, et al. Tsc1 haploinsufficiency without mammalian target of rapamycin activation is sufficient for renal cyst formation in Tsc1 $+/-$  mice. *Cancer Res*. 2006; 66:7934–8. [PubMed: 16912167]
22. Costa V, Aigner S, Vukcevic M, Sauter E, Behr K, Ebeling M, et al. mTORC1 Inhibition Corrects Neurodevelopmental and Synaptic Alterations in a Human Stem Cell Model of Tuberous Sclerosis. *Cell Rep*. 2016; 15:86–95. [PubMed: 27052171]
23. Peri S, Caretti E, Tricarico R, Devarajan K, Cheung M, Sementino E, et al. Haploinsufficiency in tumor predisposition syndromes: altered genomic transcription in morphologically normal cells heterozygous for VHL or TSC mutation. *Oncotarget*. 2016; 5



24. Xie C-Q, Zhang J, Villacorta L, Cui T, Huang H, Chen YE. A highly efficient method to differentiate smooth muscle cells from human embryonic stem cells. *Arterioscler Thromb Vasc Biol.* 2007; 27:e311–2. [PubMed: 18029907]
25. Shim B, Pacheco Rodriguez G, Kato J, Darling TN, Vaughan M, Moss J. Sex-specific lung diseases: effect of oestrogen on cultured cells and in animal models. *Eur Respir Rev.* 2013; 22:302–11. [PubMed: 23997058]
26. Parkhitko A, Myachina F, Morrison TA, Hindi KM, Auricchio N, Karbowniczek M, et al. Tumorigenesis in tuberous sclerosis complex is autophagy and p62/sequestosome 1 (SQSTM1)-dependent. *Proc Natl Acad Sci USA.* 2011; 108:12455–60. [PubMed: 21746920]
27. Taveira-DaSilva AM, Moss J. Clinical features, epidemiology, and therapy of lymphangioleiomyomatosis. *Clin Epidemiol.* 2015; 7:249–57. [PubMed: 25897262]
28. Zhe X, Schuger L. Combined smooth muscle and melanocytic differentiation in lymphangioleiomyomatosis. *J Histochem Cytochem.* 2004; 52:1537–42. [PubMed: 15557209]
29. Matsumoto Y, Horiba K, Usuki J, Chu SC, Ferrans VJ, Moss J. Markers of cell proliferation and expression of melanosomal antigen in lymphangioleiomyomatosis. *Am J Respir Cell Mol Biol.* 1999; 21:327–36. [PubMed: 10460750]
30. Gilbert ER, Eby JM, Hammer AM, Klarquist J, Christensen DG, Barfuss AJ, et al. Positioning ganglioside D3 as an immunotherapeutic target in lymphangioleiomyomatosis. *The American Journal of Pathology.* 2013; 183:226–34. [PubMed: 23665200]
31. Hoon V, Thung SN, Kaneko M, Unger PD. HMB-45 reactivity in renal angiomyolipoma and lymphangioleiomyomatosis. *Arch Pathol Lab Med.* 1994; 118:732–4. [PubMed: 8024410]
32. Finlay G. The LAM cell: what is it, where does it come from, and why does it grow? *Am J Physiol Lung Cell Mol Physiol.* 2004; 286:L690–3. [PubMed: 15003933]
33. Juvet SC, McCormack FX, Kwiatkowski DJ, Downey GP. Molecular pathogenesis of lymphangioleiomyomatosis: lessons learned from orphans. *Am J Respir Cell Mol Biol.* 2007; 36:398–408. [PubMed: 17099139]
34. Young L, Lee H-S, Inoue Y, Moss J, Singer LG, Strange C, et al. Serum VEGF-D a concentration as a biomarker of lymphangioleiomyomatosis severity and treatment response: a prospective analysis of the Multicenter International Lymphangioleiomyomatosis Efficacy of Sirolimus (MILES) trial. *Lancet Respir Med.* 2013; 1:445–52. [PubMed: 24159565]
35. Young LR, Vandyke R, Gulleman PM, Inoue Y, Brown KK, Schmidt LS, et al. Serum vascular endothelial growth factor-D prospectively distinguishes lymphangioleiomyomatosis from other diseases. *Chest.* 2010; 138:674–81. [PubMed: 20382711]
36. Cao J, Tyburczy ME, Moss J, Darling TN, Widlund HR, Kwiatkowski DJ. Tuberous sclerosis complex inactivation disrupts melanogenesis via mTORC1 activation. *J Clin Invest.* 2017; 127:349–64. [PubMed: 27918305]
37. Choo AY, Kim SG, Vander Heiden MG, Mahoney SJ, Vu H, Yoon S-O, et al. Glucose addiction of TSC null cells is caused by failed mTORC1-dependent balancing of metabolic demand with supply. *Mol Cell.* 2010; 38:487–99. [PubMed: 20513425]
38. Inoki K, Zhu T, Guan K-L. TSC2 mediates cellular energy response to control cell growth and survival. *Cell.* 2003; 115:577–90. [PubMed: 14651849]
39. Sun Y, Gu X, Zhang E, Park M-A, Pereira AM, Wang S, et al. Estradiol promotes pentose phosphate pathway addiction and cell survival via reactivation of Akt in mTORC1 hyperactive cells. *Cell Death Dis.* 2014; 5:e1231. [PubMed: 24832603]
40. Parkhitko AA, Priolo C, Colloff JL, Yun J, Wu JJ, Mizumura K, et al. Autophagy-dependent metabolic reprogramming sensitizes TSC2-deficient cells to the antimetabolite 6-aminonicotinamide. *Mol Cancer Res.* 2014; 12:48–57. [PubMed: 24296756]
41. Wu Y, Li Y, Zhang H, Huang Y, Zhao P, Tang Y, et al. Autophagy and mTORC1 regulate the stochastic phase of somatic cell reprogramming. *Nature Cell Biology.* 2015; 17:715–25. [PubMed: 25985393]
42. Wang S, Xia P, Ye B, Huang G, Liu J, Fan Z. Transient activation of autophagy via Sox2-mediated suppression of mTOR is an important early step in reprogramming to pluripotency. *Cell Stem Cell.* 2013; 13:617–25. [PubMed: 24209762]



43. McDonald ACH, Biechele S, Rossant J, Stanford WL. Sox17-mediated XEN cell conversion identifies dynamic networks controlling cell-fate decisions in embryo-derived stem cells. *Cell Rep*. 2014; 9:780–93. [PubMed: 25373912]
44. Kinnear C, Chang WY, Khattak S, Hinek A, Thompson T, de Carvalho Rodrigues D, et al. Modeling and rescue of the vascular phenotype of Williams-Beuren syndrome in patient induced pluripotent stem cells. *Stem Cells Translational Medicine*. 2013; 2:2–15. [PubMed: 23283491]
45. Shelton M, Kocharyan A, Liu J, Skerjanc IS, Stanford WL. Robust generation and expansion of skeletal muscle progenitors and myocytes from human pluripotent stem cells. *Methods*. 2016; 101:73–84. [PubMed: 26404920]
46. Hotta A, Cheung AYL, Farra N, Garcha K, Chang WY, Pasceri P, et al. EOS lentiviral vector selection system for human induced pluripotent stem cells. *Nat Protoc*. 2009; 4:1828–44. [PubMed: 20010937]
47. Zhe X. Combined Smooth Muscle and Melanocytic Differentiation in Lymphangiomyomatosis. *J Histochem Cytochem*. 2004; 52:1537–42. [PubMed: 15557209]
48. Corrin B, Liebow AA, Friedman PJ. Pulmonary lymphangiomyomatosis. A review. *The American Journal of Pathology*. 1975; 79:348–82. [PubMed: 1146965]
49. Patel B, Patel J, Cho J-H, Manne S, Bonala S, Henske E, et al. Exosomes mediate the acquisition of the disease phenotypes by cells with normal genome in tuberous sclerosis complex. *Oncogene*. 2016; 35:3027–36. [PubMed: 26434588]
50. Laplante M, Sabatini DM. mTOR signaling in growth control and disease. *Cell*. 2012; 149:274–93. [PubMed: 22500797]

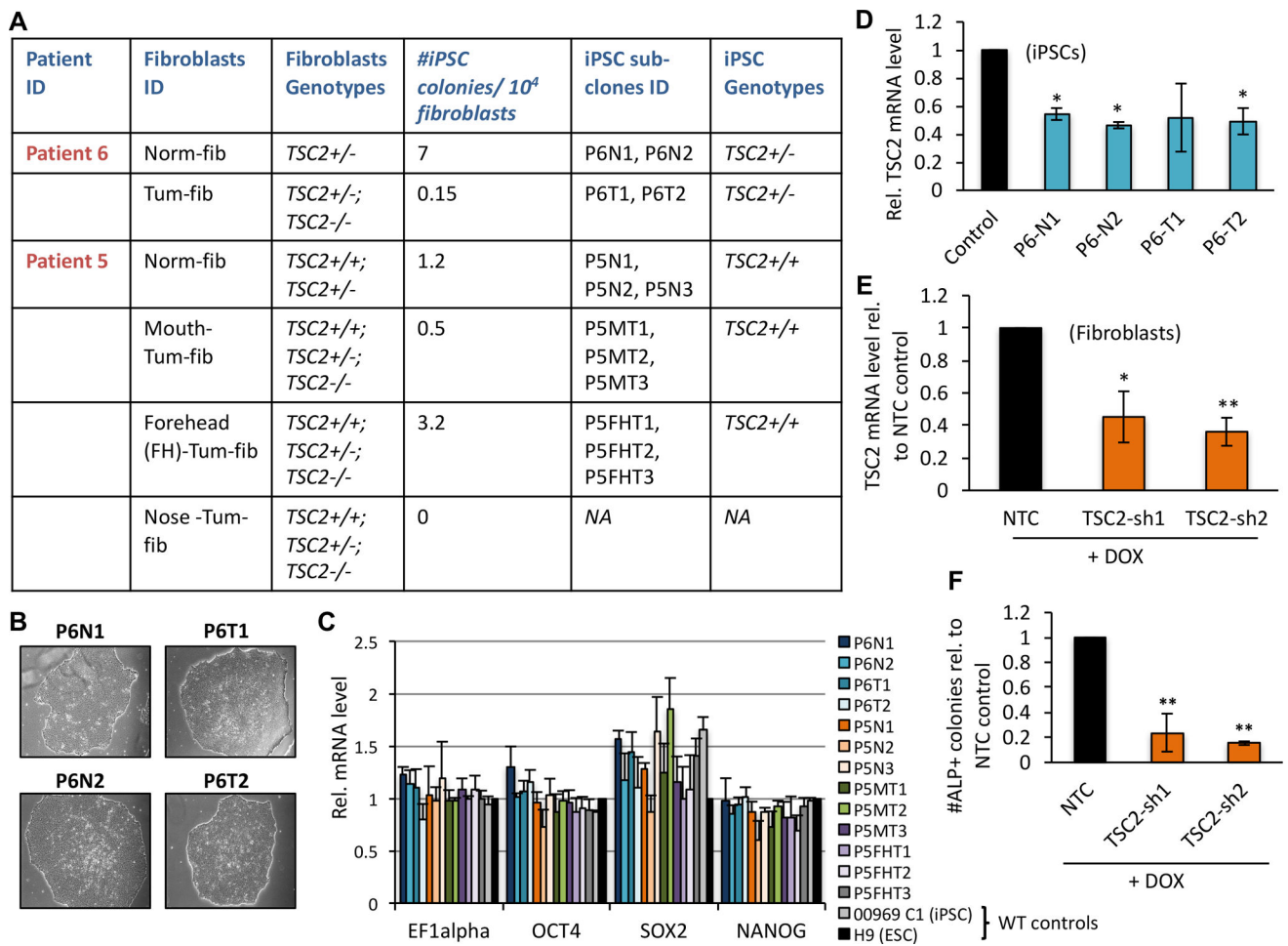


**Figure 1.**

*TSC2* deficiency inhibits iPSC reprogramming. (A) *TSC2* genotypes of patient-derived fibroblasts and derivative iPSC sub-clones used in this study, as well as frequency of iPSC reprogramming of patient-derived fibroblasts. (B) Representative phase contrast images of Patient 6 (P6)-derived iPSC colonies. (C) qRT-PCR analysis of mRNA levels of pluripotency markers (indicated along X-axis) in control and patient-derived iPSC lines, expressed as relative (Rel.) to wild type (WT) H9 ESCs for each indicated gene. (D) qRT-PCR for *TSC2* in P6-derived iPSCs relative to non-patient control cell line '168'. Relative *TSC2* expression (E) and number of alkaline phosphatase (ALP) positive iPSC colonies (F) in 090 fibroblasts carrying *TSC2* shRNAs ('TSC2-sh1' and 'TSC2-sh2') or a scrambled 'control' RNA molecule, following Dox-induced shRNA expression. Data in E and F are expressed as relative to scrambled 'control' cells. Statistics are relative to the following controls: H9 ESCs (C), 168 iPSCs (D) and scrambled controls (E, F). P values of <0.05 (\*), <0.01 (\*\*) are indicated. Three biological replicates were performed for each experiment.

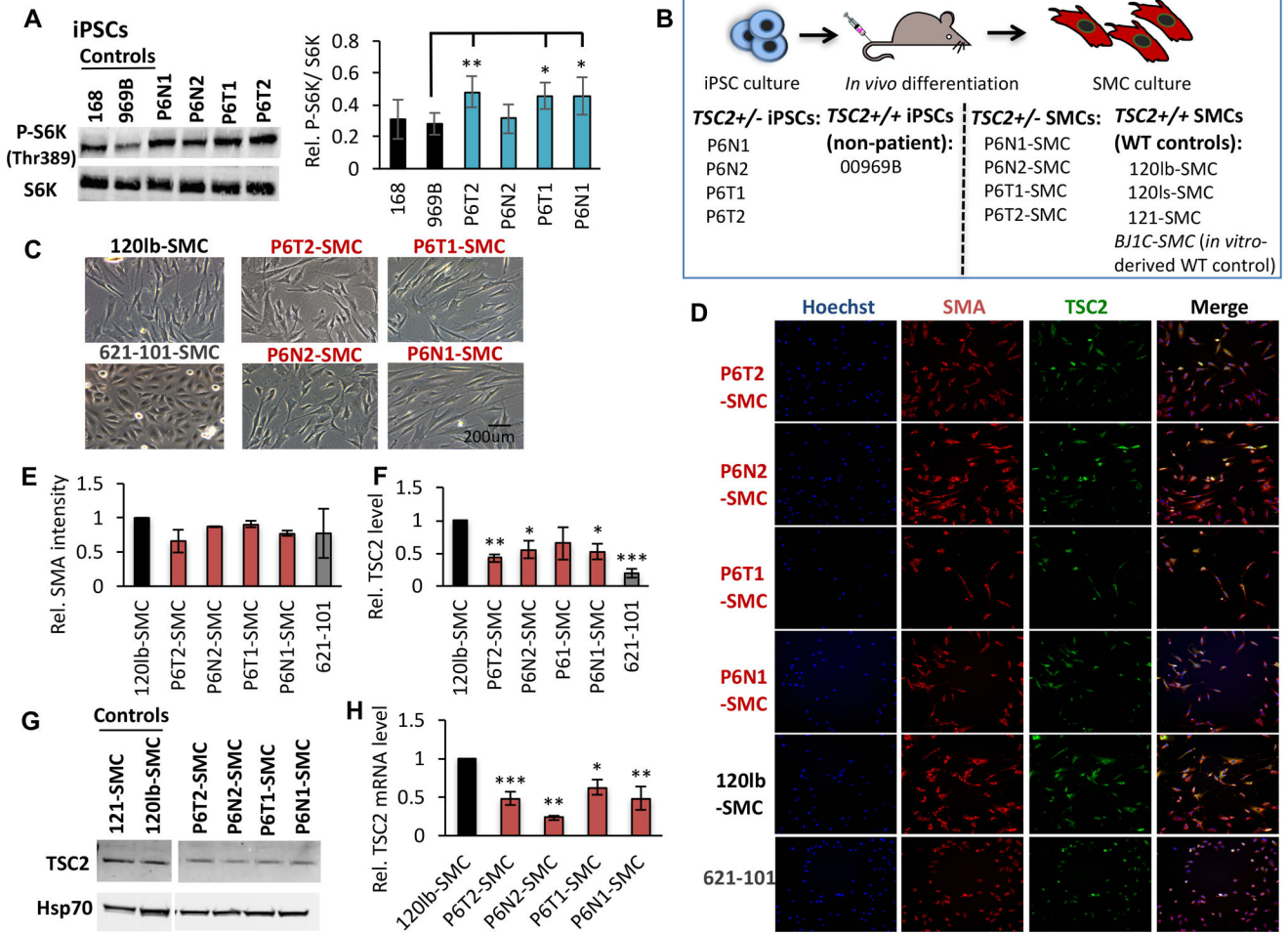


**Figure 2.** Establishment of TSC/LAM patient-derived SMC lines. (A) Representative western blot analysis and densitometry quantification, expressed as relative to control cell line 969B, of total and phosphorylated (P-S6K, Thr389) S6K in control and P6 iPSC lines. (B) Four P6 iPSC lines (as indicated), and one non-patient WT control iPSC line (969B, as indicated), were injected intramuscularly for *in vivo* differentiation in teratomas and explants were cultured under SMC growth conditions. The four SMC patient-derived lines and three SMC WT control lines that were established using this approach are indicated. Note we also use a fourth WT control SMC line in this study, BJIC-SMC, which was generated by *in vitro* differentiation of non-patient iPSCs. Representative phase contrast (C) and high content imaging (HCI) immunofluorescence (smooth muscle actin [SMA], TSC2; D) images of P6-derived, 120lb-SMC control and 621-101 cells. Quantification of HCI images for mean intensity of SMA (E) and TSC2 (F) proteins, expressed as relative to 120lb-SMC controls, as well as western blot for TSC2 (G), in cultured cell lines. (H) *TSC2* mRNA expression relative to 120lb-SMCs. Statistics are relative to 969B (A), and 120lb-SMC (E, F, H) controls. P values of <0.05 (\*), <0.01 (\*\*) and <0.001 (\*\*\*) are indicated where statistical differences were observed. A minimum of three biological replicates were performed for each experiment.

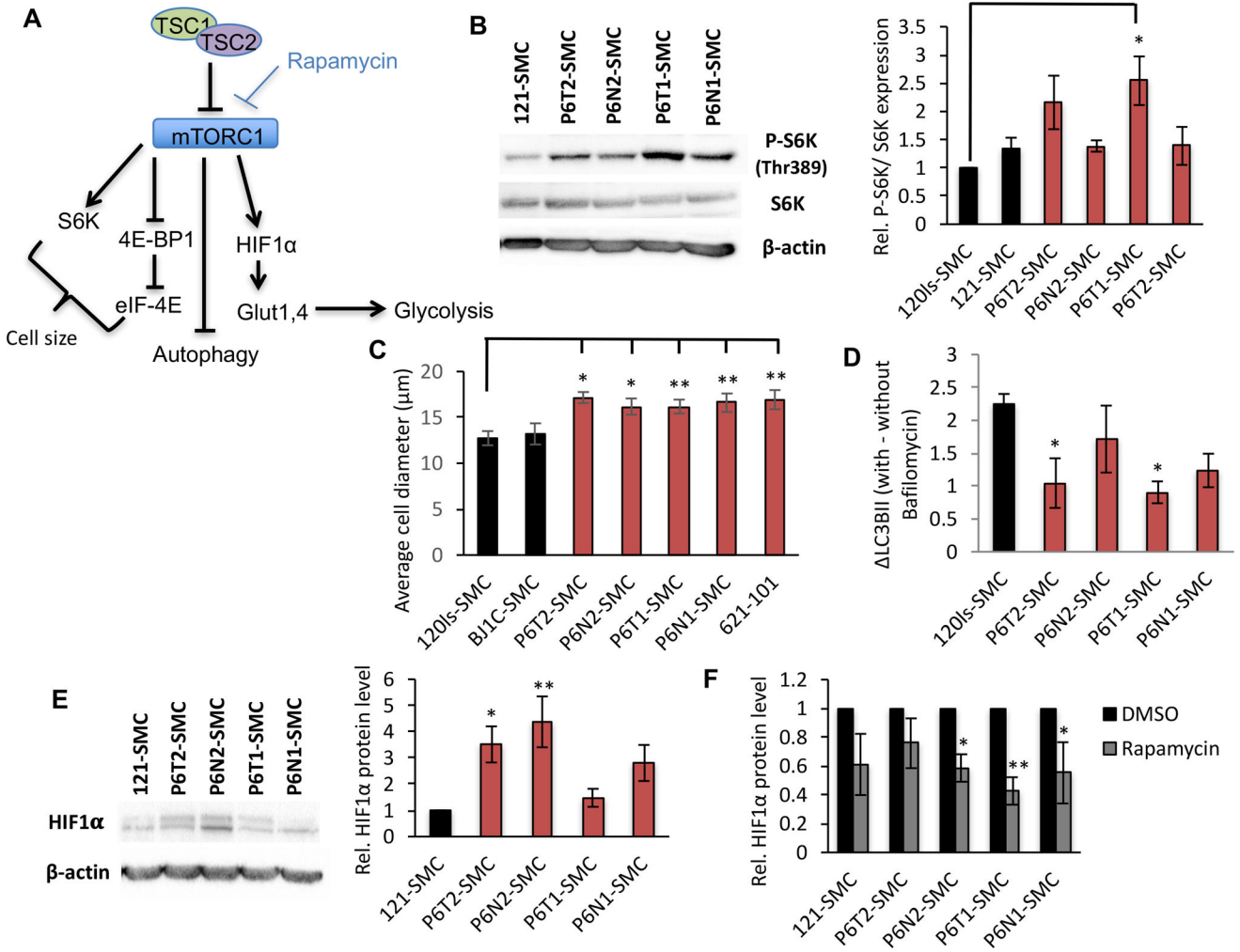


**Figure 3.** Patient-derived SMC lines exhibit hyperactive mTORC1 signaling. (A) Simplified mTORC1 signaling network. (B) Representative western blot for pan-S6K and its T389 phosphorylated form (P-S6K) in SMC lines, and densitometry based quantification expressed as relative to control 120ls-SMCs. Average diameter of cells (C) and change in LC3B-II levels with or without bafilomycin A1 (D) in SMC lines. (E) Western blot for HIF1α (left panel) and densitometry-based quantification (right panel) expressed as relative to 121-SMC control. (F) Densitometry-based quantification of western blots for HIF1α expression in SMC lines in the presence of DMSO (vehicle) or rapamycin, expressed as relative to the DMSO condition for each cell line. Statistics are relative to 120ls-SMC (B, C, D), 121-SMC (E), and DMSO condition (F) (t-test). P values of <0.05 (\*) and <0.01 (\*\*) are indicated. A minimum of three biological replicates were performed for each experiment.

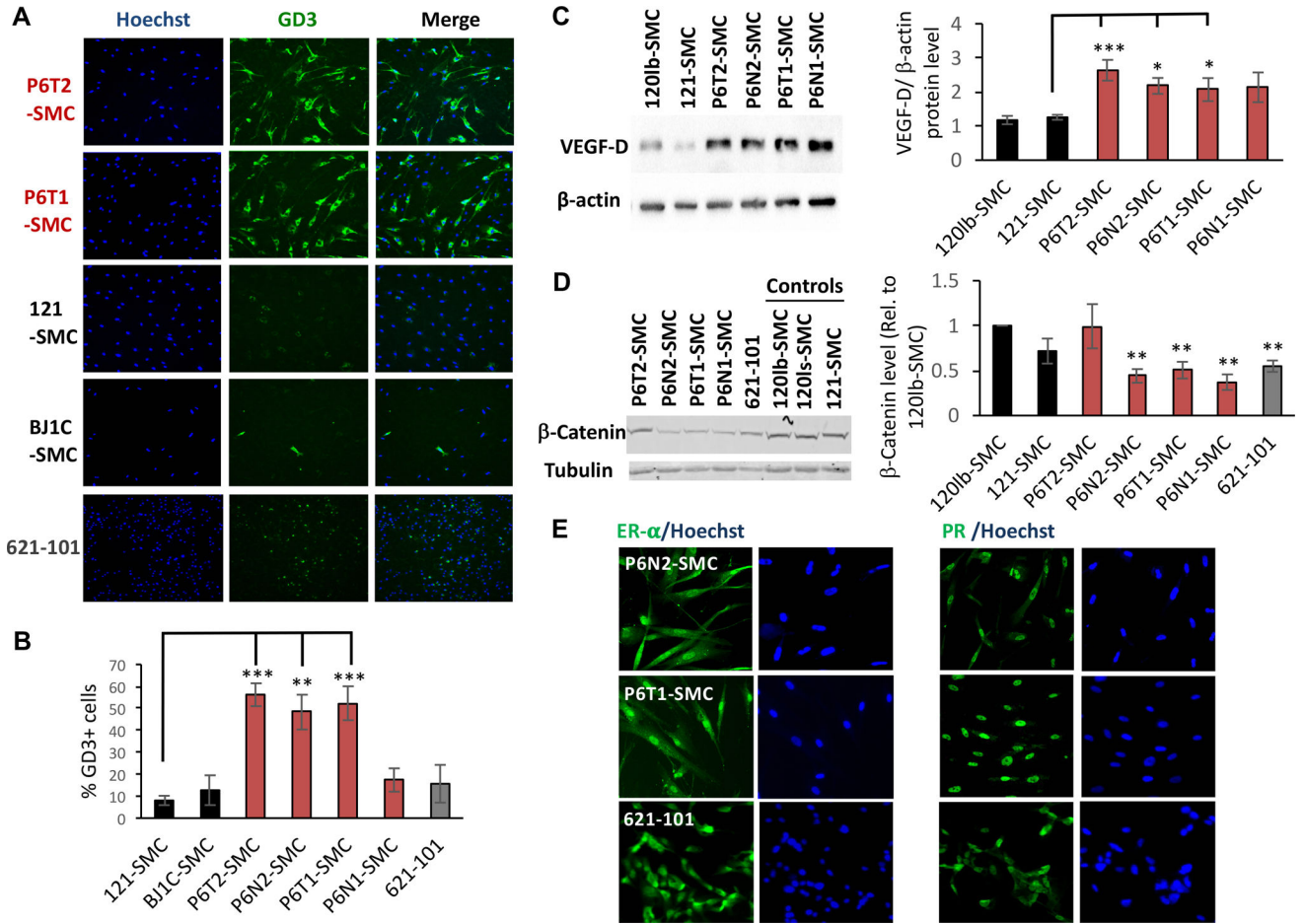


**Figure 4.** Patient-derived SMCs exhibit known LAM cell biomarkers. (A) HCI for ganglioside D3 (GD3) and Hoechst nuclear stain in control (121-SMC, BJ1C-SMC), P6-SMC, and 621-101 cell lines, with representative quantification (B). (C) Representative western blots and densitometry quantification (expressed as VEGF-D levels normalized to  $\beta$ -actin expression) for VEGF-D in P6-SMC and control (120lb-SMC, 121-SMC) lines. (D) Representative western blots and densitometry quantification (normalized to tubulin and expressed as relative to 120lb-SMC control) for  $\beta$ -Catenin in P6-SMC and control (120lb-SMC, 120ls-SMC, 121-SMC) lines. (E) Representative immunofluorescence images for estrogen receptor alpha (ER- $\alpha$ ) and progesterone receptor (PR), and the corresponding Hoechst images, in P6-SMC lines and 621-101 cells. Statistics are relative to 121-SMC (B, C), and 120lb-SMC (D) controls. P values of <0.05 (\*), <0.01 (\*\*), and <0.001 (\*\*\*) are indicated. A minimum of four and up to seven biological replicates were performed for each experiment.



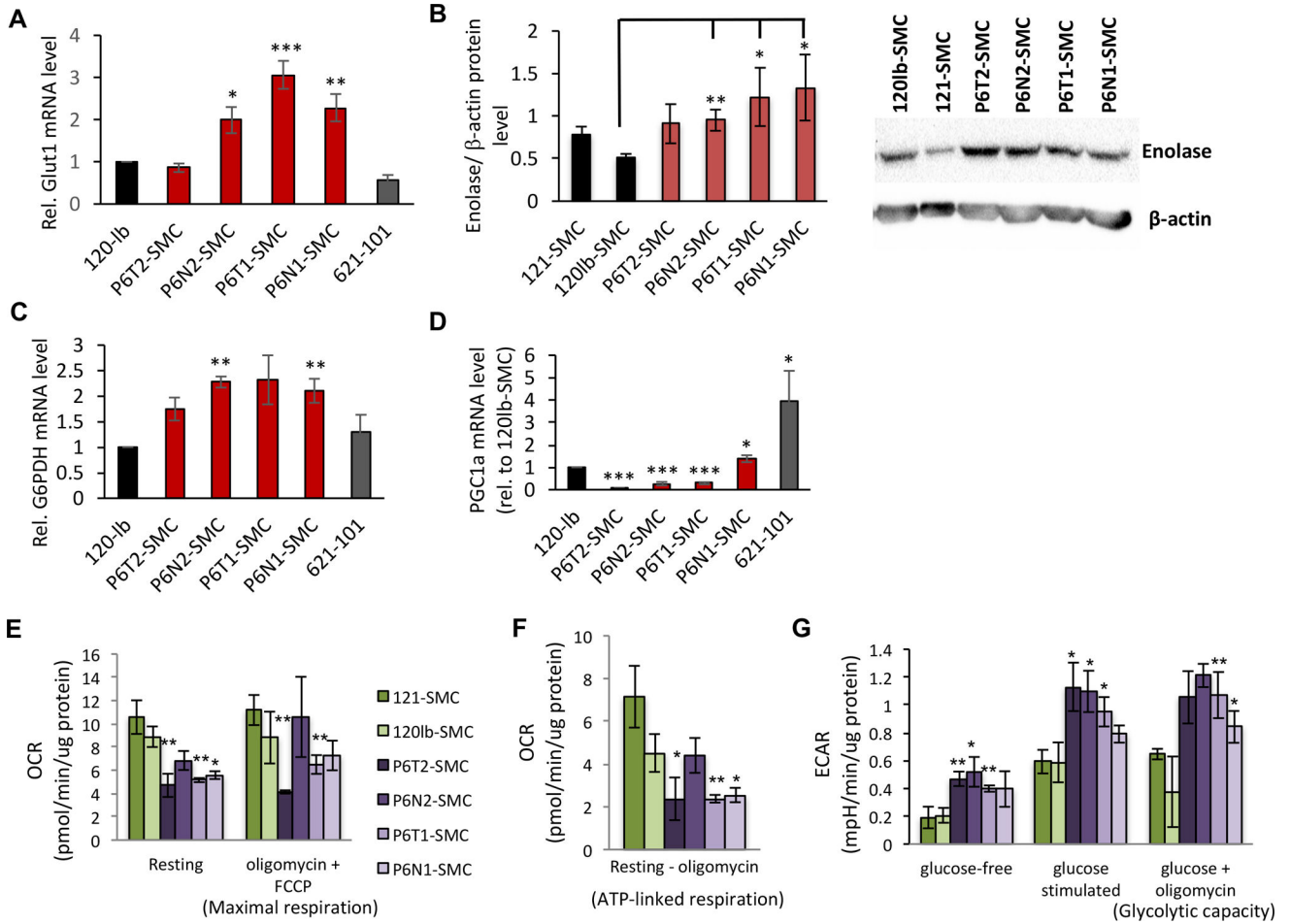


**Figure 5.** *TSC2*<sup>+/-</sup> SMCs exhibit metabolic reprogramming to a glycolytic state. (A) qRT-PCR analysis of *GLUT1* expression in SMC lines and 621-101 cells, expressed as relative to 120lb-SMC control. (B) Representative western blot (lower panel) and densitometry-based quantification (upper panel) of enolase expression (plotted are enolase levels normalized to β-actin levels) in SMC lines. qRT-PCR analysis of *G6PDH* (C) and *PGC1a* (D) expression in SMC lines (expressed as relative to 120lb control cells). Statistics for A–D are relative to the 120lb-SMC control line. Oxygen consumption rate (OCR) measurements under resting and maximal respiratory conditions (E), and the difference between OCR levels at resting state and following exposure to oligomycin to indicate ATP turnover (F). Extracellular acidification rate (ECAR) under glucose-free and maximal (+glucose, +oligomycin) conditions (G). For E–G, control (green bars) and P6-derived (purple bars) SMC lines are normalized to total protein as indicated. Statistics are relative to the average of the two control lines. P values of <0.05 (\*), <0.01 (\*\*), and <0.001 (\*\*\*) are indicated. t-tests were performed for panels B and G. A minimum of three biological replicates were performed for each experiment.



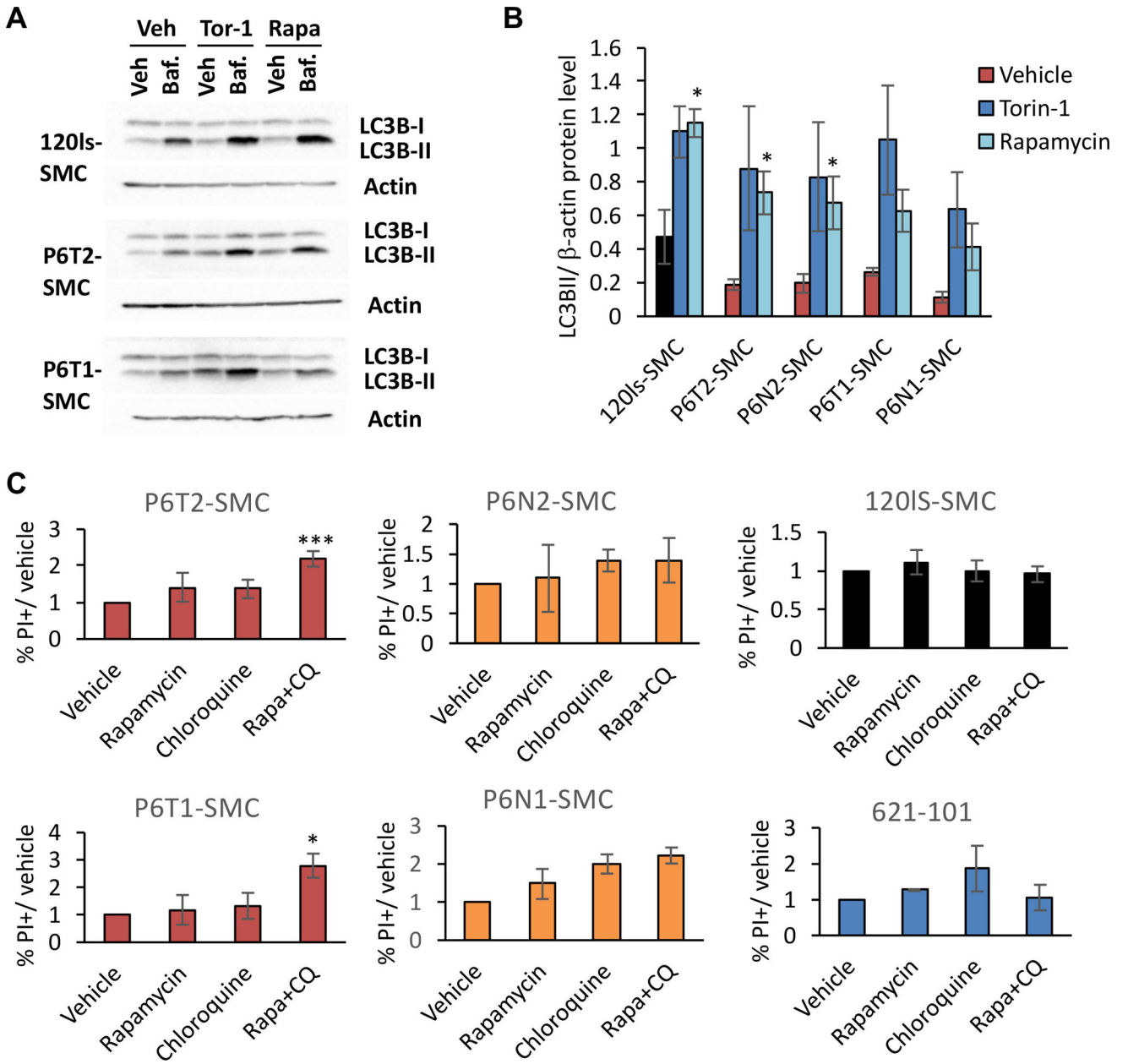


**Figure 6.** Selective toxicity of TSC-LAM patient SMCs by dual targeting of mTORC1 and autophagy signaling. (A) Representative western blots of LC3B-I and LC3B-II levels in control (120Is-SMCs) and P6-derived SMC lines to depict LC3B-II accumulation in vehicle versus +bafilomycin A1 conditions, and the corresponding response to mTOR inhibitors torin-1 and rapamycin. (B) Basal levels of LC3B-II, based on densitometry quantification of western blots and normalized to  $\beta$ -actin levels, in SMC lines under vehicle, torin-1 or rapamycin treatment. Statistics are relative to vehicle. (C) % of cells positive for propidium iodide (PI) relative to vehicle for each cell line, following a 24 hr treatment with 2.5  $\mu$ M chloroquine (CQ), 20 nM rapamycin, or both. Measurements were collected *via* flow cytometry. P values

of  $<0.05$  (\*) and  $<0.001$  (\*\*\*) , obtained by t-test, are indicated. Three biological replicates were performed for each experiment and treatment condition.

Author Manuscript

Author Manuscript

Author Manuscript

Author Manuscript

**Table 1**

Summary of LAM cell phenotypes observed in *TSC2*<sup>+/-</sup> patient-derived SMC lines and 621-101 cells. Checkmarks, x-marks, and 'ND' indicate respectively that the phenotype was observed, not observed, and not determined. '---' indicates that positive staining for gp100 was detected, but in a small sub-population of cells.

<b>Cell line ID:</b>		<b>621-101</b>	<b>P6N1-SMC</b>	<b>P6N2-SMC</b>	<b>P6T1-SMC</b>	<b>P6T2-SMC</b>
<b>TSC2 loss</b>	Reduced TSC2 expression	✓	✓	✓	✓	✓
	SMC marker expression	✓	✓	✓	✓	✓
<b>LAM/ TSC markers</b>	Elevated GD3 levels	x	x	✓	✓	✓
	Elevated VEGF-D levels	x	x	✓	✓	✓
	Aberrant $\beta$ -Catenin expression	✓	✓	✓	✓	x
	ER- $\alpha$ , PR expression	✓	✓	✓	✓	✓
	gp100 expression	---	---	ND	---	---
	Increased P-S6/ P-S6K, cell size	✓	✓	✓	✓	✓
<b>mTOR activation</b>	Rapamycin responsiveness	✓	✓	✓	✓	✓
	Glycolytic metabolism	ND	✓	✓	✓	✓
	Reduced autophagy	ND	✓	x	✓	✓
	Sensitivity to mTOR + autophagy inhibition	x	x	x	✓	✓